

CONTROL OF ASH DEPOSITION THROUGH THE HIGH TEMPERATURE ADSORPTION OF ALKALI VAPORS ON SOLID SORBENTS

Wayne A. Punjak, Mohit Uberoi and Farhang Shadman
Department of Chemical Engineering
University of Arizona
Tucson, AZ 85715

INTRODUCTION

Coal usually contains sodium and potassium minerals in various chemical and physical forms. During the combustion or gasification of coal, much of this alkali is released into the gas phase. This vapor is usually in the form of alkali chlorides. In the presence of sulfur, alkali sulfates are also formed. This alkali condenses on and reacts with ash to form low melting point phases that enhance fouling¹.

Cleaning of coal removes some of the alkali but is not effective enough to decrease the alkali concentration to acceptable levels. A promising technique for the removal of alkali from hot flue gases is by using materials (sorbents) that will adsorb and/or react with alkali vapors. In general, the sorbents can be used in two ways. One method is by passing the alkali-laden flue gas through a fixed bed of an appropriate sorbent. This process has been considered for alkali removal from flue gases in the combined-cycle power generation from coal^{2,3,4}. The second method is the injection of sorbents with coal for the in-situ capturing of alkali during pulverized coal combustion. This method has received much less attention⁵.

The choice of a suitable sorbent depends on the coal properties and the process operating conditions. In general, however, the important characteristics desired in a potential sorbent are high temperature compatibility, rapid rate of adsorption, high loading capacity, transformation of the alkali into a less corrosive form and irreversible adsorption to prevent the release of adsorbed alkali during process fluctuations.

Previous studies in this laboratory^{6,7} and those of other investigators^{2,3,4,8} have suggested that bauxite, kaolinite and emathlite are promising alkali vapor sorbents. The purpose of this study is to obtain fundamental information on the kinetics and the mechanism of alkali adsorption on these sorbents.

EXPERIMENTAL APPROACH

The composition of the sorbents used in this study are given in Table 1. These sorbents were used in the form of thin flakes with the approximate thickness of 0.5 mm. The flakes were devolatilized and then stored under vacuum until used.

The apparatus used in the sorption experiments consisted of a tubular quartz reactor, an electronic microbalance and a movable electric furnace. A detailed description of this system is given elsewhere^{6,9}. The experiments were performed in two groups. The first set of tests were made at a sorbent temperature of 800°C under a flowing simulated flue gas (SFG) atmosphere. The composition of the SFG was 80% N₂, 15% CO₂, 3% O₂ and 2% H₂O with a flowrate of 150 or 200 scfm, depending on the experiment involved. Crystalline NaCl was used as the alkali source. The alkali vapor concentration was varied between 50 and 230 ppmv, well below saturation to avoid physical condensation.

In these experiments, sorbent flakes were suspended from the microbalance directly above the alkali source which was placed in the bottom of the quartz reactor. The SFG was passed over the alkali source to vaporize and transport it toward the sorbent. A second SFG line, split from the first, entered the reactor a few cm above the first one and was used to dilute the alkali vapor to a desired concentration. A few cm above the sorbent the gases mixed with purging nitrogen coming down from the microbalance and went out an exhaust port. Thermocouples were placed on the outside of the reactor near the alkali source and the sorbent to monitor the temperature of each.

In the second set of tests the alkali source, either NaCl, KCl or K_2SO_4 , was allowed to saturate the simulated flue gas in the vicinity of the sorbent. The temperature in these experiments was varied from 750 to 1135°C. Thermodynamic calculations showed that for all of these experiments, essentially all of the alkali in the vapor phase remains in the form of the salt from which it was vaporized (i.e., NaCl, KCl or K_2SO_4).

EXPERIMENTAL RESULTS

Typical experimental weight gain profiles for the three sorbents tested in the first set of experiments are shown in Figure 1. The results indicate a decrease in adsorption rate with loading and a final alkali saturation limit. Bauxite is observed to have the highest initial rate, while kaolinite has the largest capacity. The effect of varying the alkali vapor concentration on the weight gain profiles for each sorbent was also tested. Typical profiles for kaolinite are shown in Figure 2. It can be seen that an increase in the alkali concentration results in an increase in the adsorption rate.

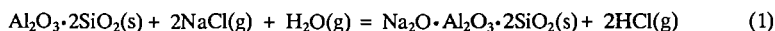
An important difference between the adsorption characteristics of the three sorbents is the reversibility of the adsorption process. After saturation, the reversibility of the alkali uptake was tested for each sorbent by reducing the alkali vapor concentration to zero. No desorption was observed for kaolinite and emathlite, but bauxite lost approximately 10% of its total initial weight gain. This suggests that the mechanism of adsorption is not the same for the three sorbents.

The fresh devolatilized and fully saturated sorbents were analyzed using various chemical analytical techniques to gain further insight into the mechanism of alkali sorption. Scanning Auger microscopy (SAM) was performed on the samples to determine elemental composition and alkali distribution. One important difference between the substrates revealed by these results is in the ratio of sodium to chlorine adsorbed. Chlorine, which has a peak at 176 eV, was not observed in the products of adsorption on emathlite and kaolinite. In contrast, chlorine was partially retained by bauxite.

The cross sections of partially converted samples were mapped for alkali using SAM to study the changes in the substrate during adsorption. The alkali content was observed to be largest near the outer edge of the flake, decreasing rapidly toward the flake center. Similar results were obtained for bauxite and emathlite, indicating that the sorption kinetics for all three sorbents are influenced by intraphase diffusion under the experimental conditions used. Additional details can be found in another publication¹³.

X-ray diffraction (XRD) spectra obtained for the sorbents prior to and after alkali adsorption indicate the formation of several reaction products. Kaolinite saturated with sodium from NaCl

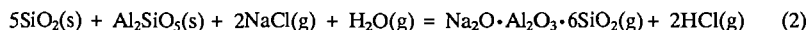
was found to contain primarily nephelite and carnegieite, sodium aluminosilicate polymorphs with the chemical formula $\text{Na}_2\text{O}\cdot\text{Al}_2\text{O}_3\cdot 2\text{SiO}_2$. In nephelite, which is thermodynamically favored at high temperatures, the sodium cation is octahedrally coordinated and in carnegieite it is tetrahedrally coordinated¹⁰. Based on this information and the absence of chlorine in the adsorption product, the following reaction scheme is proposed:



where metakaolinite ($\text{Al}_2\text{O}_3\cdot 2\text{SiO}_2$) is the dehydration product of kaolinite. The stoichiometry of this reaction suggests a 27.9% increase in sample weight on complete conversion. This is very close to the observed 26.6%. In addition, the alkali uptake determined by atomic emission analysis is very close to that predicted by Reaction 1. Kaliophilite ($\text{K}_2\text{O}\cdot\text{Al}_2\text{O}_3\cdot 2\text{SiO}_2$), the potassium analog of nephelite, was observed as the reaction product of KCl and K_2SO_4 with kaolinite. Other investigators^{10,11} also observed the formation of nephelite and kaliophilite when mixtures of sodium and potassium compounds, respectively, were heated with kaolinite to high temperatures. Due to the relatively high melting points of nephelite and kaliophilite, kaolinite would be a suitable sorbent for the in-situ capture of alkali at high temperatures. It is also an excellent choice for the downstream removal of alkali because of its high capacity.

The XRD spectra for the other sorbents indicate a more complicated process. The spectrum for as-received bauxite shows the presence of alpha-quartz, corundum and hematite. The XRD results for fully saturated bauxite indicate the formation of nephelite and carnegieite produced by a reaction similar to Reaction 1 in which NaCl was used as the alkali source. However, the amount of silica in bauxite is not sufficient for Reaction 1 to account for all the adsorbed alkali. Apparently, the rest of the alkali is present as glassy products or physisorbed chloride not detectable by XRD. Since chlorine is lost from the saturated bauxite during desorption, physisorbed NaCl might be the portion which is removed during the desorption experiments. The non-dissociative adsorption of alkali chlorides on alumina has been reported previously^{7,12}. Hematite, present both before and after adsorption, did not undergo any noticeable transformation.

The XRD results for emathlite show the presence of aluminosilicate (Al_2SiO_5), alpha quartz and cristobalite before adsorption. The sample fully saturated with sodium from NaCl consisted primarily of albite ($\text{Na}_2\text{O}\cdot\text{Al}_2\text{O}_3\cdot 6\text{SiO}_2$) together with smaller amounts of sodium calcium aluminate ($\text{NaCa}_4\text{Al}_3\text{O}_9$). Therefore, much of the sodium capture by emathlite can be described by the following overall reaction:



Since albite has a relatively low melting point (1000°C), it is more suited to downstream alkali removal where the flue gas temperature is lower.

MATHEMATICAL MODEL

A mathematical model was formulated to describe the simultaneous physical and chemical processes that occur during alkali sorption by solid sorbents. A brief description of the model is given here. Additional details are given in another publication¹³. In this formulation the alkali

compound, A, diffuses through the porous sorbent and is then adsorbed upon contact with the sorbent surface. The adsorption process is a combination of physical adsorption and reaction, the details of which depend on the alkali and substrate. Assuming a quasi-steady state for diffusion and reaction in a porous particle, the conservation equation for alkali vapor can be written as follows:

$$\nabla \cdot D_e \nabla C_A = R_A \quad (3)$$

where R_A is the molar rate of adsorption of alkali per unit bulk volume of sorbent. The boundary conditions used to solve Equation 3 are a zero concentration gradient at the flake center and an equation of fluxes at the flake surface. The local alkali loading or alkali concentration in the solid phase, C_s , is given by the following conservation equation:

$$(1 - \epsilon_0) \frac{\partial C_s}{\partial t} = R_A \quad (4)$$

in which ϵ_0 is the initial porosity. The initial condition used to solve Equation 4 is $C_s = 0$ at $t = 0$. It is assumed that the local rate of adsorption is given by the following rate expression:

$$R_A = (1 - \epsilon_0) k C_A \left(1 - \frac{C_s}{C_{sf}}\right) \quad (5)$$

in which k is the overall rate coefficient and C_{sf} is the alkali concentration in the solid phase at sorbent saturation. In this formulation the porosity is allowed to vary with conversion. Equation 3 was solved numerically using a variable-step central-difference technique. Equation 4 was solved simultaneously to obtain the solid conversion. The overall loading at any time is obtained by integrating C_s over the sorbent volume.

The model was first used to extract intrinsic kinetic information from the weight gain profiles. The overall rate constant, k , for each sorbent was obtained by fitting the model to the initial rate data. These rate constants together with the other parameters were then used to predict weight gain profiles for the other three sorbents at different alkali concentrations. The profiles and model predictions for emathlite are given in Figure 5.

The values of the rate coefficients estimated from the model are given in Table 2. The difference in the rate coefficients shows that the adsorption process is not a physical and nonselective process, but rather a chemical process which depends on the chemical nature of the sorbent. Under the experimental conditions used, this model suggests that sorbent particles smaller than $50 \mu\text{m}$ must be used for interphase and intraphase diffusional resistances to have a negligible influence on the observed sorption kinetics.

Evaluation of the experiments performed under saturated vapor conditions was more complicated. The data for these experiments are given in Table 3. Although no desorption of alkali was observed for kaolinite in the previous set of experiments, it was possible to desorb a portion of the alkali in the saturated vapor experiments. This suggests that in addition to chemical reaction, alkali was physically condensing on the sorbent. This can be explained by the Kelvin effect which predicts that the alkali vapor was supersaturated in the sorbent pores under the experimental conditions used. The model described above does not consider the physical condensation of alkali and therefore can not be used to evaluate the data in these runs. This model is currently being modified to allow for the physical condensation and chemical reaction of alkali.

CONCLUSIONS

It was found that kaolinite, bauxite and emathlite are suitable sorbents for the removal of alkali vapors from hot flue gases. However, kaolinite and bauxite are more suitable than emathlite at temperatures above 1000°C. The rate of adsorption was observed to decrease with alkali loading and drop to zero when a final saturation limit is achieved. This saturation limit is the highest for kaolinite. The adsorption of alkali chloride on kaolinite and emathlite is irreversible with the release of chlorine back to the gas phase as HCl vapor. The adsorption on bauxite is partially reversible and a portion of the chlorine is retained. Under the experimental conditions used it was found that interphase and intraphase diffusional resistances influence the kinetics of the adsorption process. The proposed theoretical model agrees with the experimental data and can be used for design and parametric studies if the alkali vapor concentration is well below saturation levels. Near saturation, a model must be used that allows for the physical condensation of alkali and reaction with the sorbent.

REFERENCES

1. Borio, R.W.; Levasseur, A.A., "Mineral Matter and Ash in Coal," Vorres, K.S. ed.; ACS Symposium Series, ISSN 0097-5156; 301; chapter 21 (1986).
2. Bachovchin, D.M.; Alvin, M.A.; DeZubay, E.A.; Mulik, P.R., "A Study of High Temperature Removal of Alkali in a Pressurized Gasification System," DOE-MC-20050-2226; Westinghouse Res. Dev. Center: Pittsburgh, PA (1986).
3. Jain, R.C.; Young, S.C., "Laboratory/Bench Scale Testing and Evaluation of A.P.T. Dry Plate Scrubber," DOE-ET-15492-2030; Air Pollution Technology, Inc.: San Diego, CA (1985).
4. Lee, S.H.D.; Johnson, I., *J. Eng. Power*, 102, 397 (1980).
5. Shadman, F.; Peterson, T.W.; Wendt, J.O.L.; Punjak, W.A.; Rizeq, R.G., "Mechanism of Surface Enrichment and Adhesion of Coal Combustion Particulates," second quarterly report; DE-FG22-86PC90505; US DOE (PETC) (1987).
6. Punjak, W.A.; Shadman, F., *Energy and Fuels*, 2 (5), 702 (1988).
7. Shadman, F.; Punjak, W.A., "Solid Adsorbents for the Control of Alkali in Combustion Systems," paper presented at the Fall meeting of Western States Section, Combustion Institute, Tucson, AZ (1986).
8. Lee, S.H.D.; Henry, R.F.; Myles, K.M., "Removal of Alkali Vapors by a Fixed Granular-Bed Sorber Using Activated Bauxite as a Sorbent," CON-8503513; Argonne National Laboratory: Argonne, IL (1985).
9. Punjak, W.A., "High Temperature Interactions of Alkali Vapors with Solids During Coal Combustion and Gasification," Ph.D. Dissertation, University of Arizona (1988).

11. Kuhn, L.; Plogmann, H., *Fuel*, **62**, 205 (1983).
12. Luthra, K.L.; LeBlanc, O.H., *J. Phys. Chem.*, **88**, 1896 (1984).
13. Punjak, W.A.; Uberoi, M.; Shadman, F., "High Temperature Adsorption of Alkali Vapors on Solid Sorbents," submitted for publication to *AIChE Journal* (1988).

Table 1
Composition of As-received Sorbents

<u>Component</u>	<u>Bauxite¹</u> <u>(wt%)</u>	<u>Kaolinite²</u> <u>(wt%)</u>	<u>Emathlite³</u> <u>(wt%)</u>
SiO ₂	11.0	52.1	73.4
Al ₂ O ₃	84.2	44.9	13.9
Fe ₂ O ₃	4.8	0.8	3.4
TiO ₂	----	2.2	0.4
CaO	----	----	5.0
MgO	----	----	2.6
K ₂ O	----	----	1.2
Na ₂ O	----	----	0.1

1. Alcoa (Paranam)
2. Burgess Pigment Company
3. Mid-Florida Mining Company

Table 2
Overall Rate Coefficients

<u>Rate Constant (units)</u>	<u>Bauxite</u>	<u>Kaolinite</u>	<u>Emathlite</u>
k [cm ³ gas/(cm ³ solid - h)]	6.1 x 10 ⁷	2.1 x 10 ⁷	5.9 x 10 ⁷
k _s [cm ³ gas/(cm ² surface area - h)]	28	9.4	37

Table 3

Initial Rate Data for Saturated Vapor Runs

Alkali	Sorbent	Alkali Vapor T (°C)	Initial Concentration ppmv	Rate (h ⁻¹)
NaCl	kaolinite	750	130	0.0349
NaCl	kaolinite	795	400	0.363
NaCl	kaolinite	875	1690	0.418
K ₂ SO ₄	kaolinite	985	5.5	0.0044
K ₂ SO ₄	kaolinite	1060	25	0.0088
K ₂ SO ₄	kaolinite	1135	270	0.0160
K ₂ SO ₄	bauxite	985	5.5	0.0073
K ₂ SO ₄	bauxite	1060	25	0.0205
K ₂ SO ₄	bauxite	1135	270	0.0403

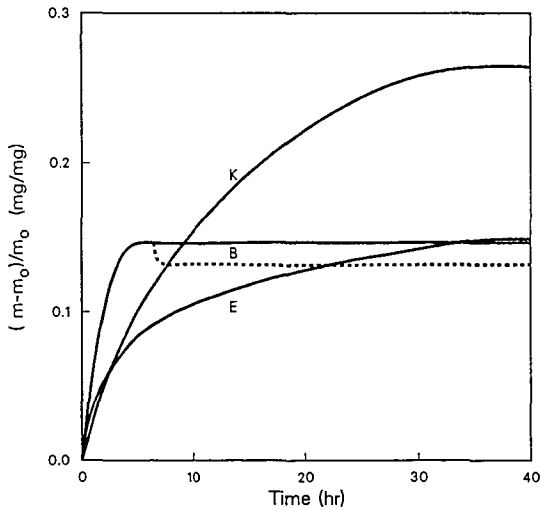


Figure 1. Temporal profile of NaCl adsorption on sorbents.
 K: kaolinite, 230 ppmv Na; B: bauxite, 185 ppmv Na;
 E: emathlite, 150 ppmv Na.

———— adsorption; - - - - - desorption.

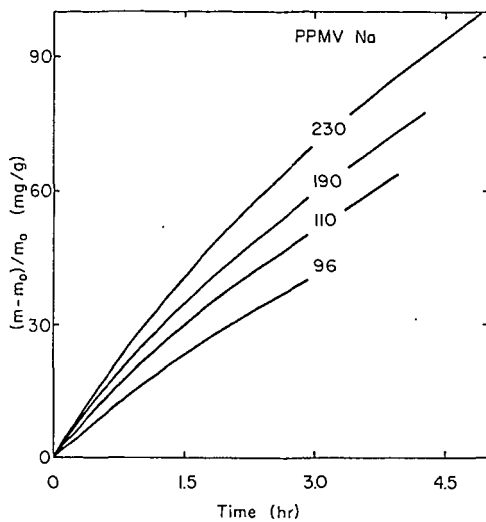


Figure 2. Temporal profile of NaCl adsorption on kaolinite.

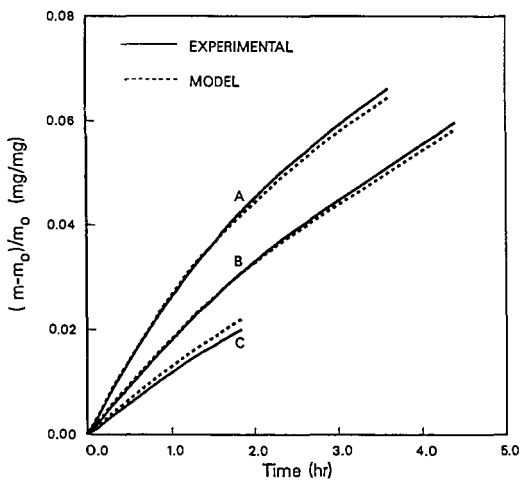


Figure 3. Comparison of model and data for NaCl adsorption on emathlite.

C_{Ab} is 125 ppmv for A, 80 ppmv for B and 65 ppmv for C.

DEPOSIT REMEDIATION IN COAL-FIRED GAS TURBINES THROUGH THE USE OF ADDITIVES

Clifford L. Spiro, C. C. Chen(*), S. Gene Kimura, Raymond G. Lavigne, and Paul W. Shields (**)

GE Corporate Research and Development Laboratory P.O.Box 8 Schenectady, NY 12345

(* Current address E.I. DuPont, Towanda, PA. (** Current address Arizona State Univ, Dept of Geology, Tempe, AZ.

ABSTRACT

Deposit formation represents a key impediment to the eventual commercialization of a direct coal-fired gas turbine engine. Deposits result from the thermal decomposition of coal-borne mineral matter followed by impact and adhesion along the hot gas pathway.

One strategy for deposit abatement is hot gas cleanup to remove particulate before entering the turbine. An alternative strategy, described in this Paper, is to modify the mineral matter/ash chemistry to render it non-adherent through the use of additives. In this way, the complexity and expense of hot gas cleanup is obviated. To date, alumina, boehmite, and a variety of kaolin clay additives have been tested in a coal-water mixture fired gas turbine simulator. A washed kaolin clay has proved to be most effective in reducing airfoil deposition. A mechanism involving in-situ slag decomposition, exsolution, and spontaneous spalling is proposed.

INTRODUCTION

A key objective of the Advanced Coal Fueled Gas Turbine Systems Program, a U.S. Department of Energy initiative, is to develop the technological basis necessary for subsequent commercial development of a direct-fired gas turbine power system. The system concept described in this paper uses a GE LM500 advanced aeroderivative gas turbine engine designed for direct firing of coal fuel. This system can be used in transportation and small stationary power applications. Components and systems required to achieve this objective in a cost-effective and environmentally sound manner are being developed.

Previous work Ref. 1-6, 9-16, reported in the open literature indicates that deposition represents a potential impediment to the commercialization of the coal-fueled gas turbine. Deposits reduce engine efficiency, and require potentially costly maintenance and down-time. Deposition is a prerequisite to hot corrosion (France, 1984).

In order to eliminate deposition, one or more of the key steps in deposition process must be interrupted. These steps are potentially system and fuel dependent, representing the complex interplay of fluid mechanics and thermochemistry.

In general, deposition can be considered as a sequence of events consisting of particle arrival and adherence. Potential mechanisms have been reviewed (Ref. 1). Applicable mechanisms for the in-line annular combustion system are the subject of this investigation, and are probably unrelated to off-board slagging systems (Ref. 2) which have distinctly different time/temperature/flow profiles, and where pre-expansion ash/slag removal is under investigation.

In order to minimize ash particle arrival rates, coal is micronized to comminute mineral matter deposit precursors, and is beneficiated to reduce the overall quantity of ash present in the system. Mineral matter occurs in coal as finely disseminated grains which melt during combustion. Presumably, if there is less mineral matter in the coal, there will be less to adhere. Complete de-ashing of the coal is not yet economically feasible. By micronizing the coal, mineral grains are also comminuted. Finer ash particles are more likely to follow hot gas path streamlines (Ref 16) and avoid impaction on the airfoils. Other mechanisms for deposition of fine particles are applicable (Ref. 8). Much of the ash remains weakly adhered to unburned char surfaces which results in larger effective Stokes diameters and impaction tendencies. To the extent that good atomization and

combustion efficiencies are achieved, this will be minimized.

Once the particles approach the airfoil surfaces, they can undergo collisional impact. To adhere, the particle kinetic energy must be at least partially dissipated, or it will not stick. By cooling the target, the molten slag which comprises the ash will freeze in the boundary layer, greatly reducing its stickiness and tendency for inelastic adhesion.

Unburned carbon will have a deleterious effect on the deposition tendency of the ash, reducing its melting point and also generating heat even after deposition. Unburned carbon has not been detected in deposits, but samples obtained by quenching combustion products (figure 1) reveal 10-40% of the combustion products consist of unburned carbon, even for combustion efficiencies in excess of 99.5%. Presumably final burnout takes place on the airfoil surface. In addition, carbon shell fragmentation may serve to dissipate particle translational energy. Improved burnout and reduced shell size are desirable, and are enhanced by improved atomization of slurry (Staub, 1988).

The condition of the target surface will also influence deposition. If it is cold and clean, there will be a limited tendency for inelastic collisions by the ash. If it is covered with a porous and fluffy surface, collisions may collapse the suprastructure and increase deposition. A very weak deposit may be eroded by incoming combustion products. A viscous liquid on the surface will very efficiently capture particles. In the event of extreme viscosity, the capture may be reduced as the surface may appear to be solid to the products of combustion.

Once deposited, the particles can be re-entrained by erosion, or may be sintered or even completely fused into a liquid. Kuczynski (Ref. 7) showed that sintering of glassy particles is governed by viscous flow. Deposit chemistry and temperature (Ref. 8) therefore determine sintering rate. A weakly sintered deposit initially develops which is subject to erosion or on-line abrasive cleaning, but eventually will fuse to a tenaciously adherent mass.

By understanding the chemistry and mechanism of deposition, the best means for deposit prevention or remediation may be identified.

EXPERIMENTAL

Coal-water mixture was provided as a 50% slurry by Otisca Industries. A summary of the slurry properties appears in Table 1. For the first four kaolin tests, an air classified kaolin was used in both a dry powder and a 70% slurry form. The dry powder was slurred with water and Colloid 211 sodium polyacrylate surfactant. Kaolin slurry was added slowly with stirring to pre-mixed coal slurry, and stirred for 1 hr. prior to combustion. The amount of kaolin was 0.8% by weight of dry coal. The kaolin contained mostly kaolinite with traces of anatase (TiO₂). Atomic absorption spectroscopy also revealed 1000ppm sodium on a slurry basis with comparable amounts of potassium anticipated.

Analytical data on deposits (vide infra) suggested that sodium was responsible for the more severe deposition. In order to limit its participation, a highly beneficiated kaolin, Satintone V* was used. It has a mean particle diameter of 0.8 microns and was mixed as a 46% slurry with Colloid 111 ammonium polyacrylate surfactant. Centrifugation of the slurry at 7000 rpm for 2 hr yielded a supernatant liquor with soluble sodium content of 2.8 ppm as determined by inductively coupled plasma emission spectroscopy. Thus the impact of alkali in such low concentrations could be minimized.

Alpha alumina, Alcan A16SG was also employed as an additive, with a primary particle size of 0.5 microns, and a surface area of 8.229 meters squared/gram. The alumina was dispersed with either Colloid 211 sodium polyacrylate, or Darvan C polyelectrolyte.

* Registered Trademark of Englehard Corporation

Boehmite has the formula $\text{AlO}(\text{OH})$, occurring in the gamma orthorhombic form. It has true density of 3 g/cc, and a hardness of 3.5-4 on Moh's scale, or roughly that of calcite. It is available in ultrapure form (no detectable alkali) as a byproduct of the Ziegler process for making alpha-olefins and fatty alcohols.

The actual boehmite used in the testing was Catapal A, a dry flowable powder which consists of 30-50 angstrom boehmite crystals which had been spray-dried to 30-50 micron granules. While complete dispersion of the crystals is possible under mildly acidic conditions, it was deemed undesirable since complete dispersions greater than 2% by weight will gel. On the other hand, the as-received grains were considered to be too coarse, representing a potential source of erosion in the event that sintering took place in the gas stream. However unlikely this might seem, precautionary comminution was performed in a mullite lined dry ball mill, using a charge of 50% volume 1" cylindrical alumina media for not less than 24 hrs. Sedimentation equivalent spherical diameter of the milled grains had a mean of 0.6 microns, considered to represent an acceptable risk of erosion, as was borne out.

Slurry was burned in the turbine simulator with no special measure taken to accommodate the presence of additives. Numerous combustion trials with doped slurry were made over a period of several months, with a typical test duration of 4-30 hr. Test conditions included the LM500 simulator, Figure 2, a 2000F firing temperature, a chamber pressure of 130 psig and the atomizing air pressure ratio maintained at 1.9. Oil assist was set at 10% to minimize complications due to combustion instability. In actuality, combustion instability did occur in the initial testing due to excessive atomizing air temperature, but this was corrected at the latter stages of testing.

Deposition rates are obtained on line through the determination of Normalized Nozzle Area Index Number (NAIN). NAIN is an indirect measure of the critical throat area between the airfoils. As deposits build up, the throat area is reduced, effectively reducing the mass flow at constant chamber pressure and temperature. By directly measuring these parameters, the NAIN can be calculated (Kimura, 1987).

RESULTS AND DISCUSSION

In the absence of additives, deposit formation is initially high, and after 25-40 hr, becomes catastrophic. (References) Figure 3 shows deposits from untreated Blue Gem coal after 20 and 45 hr respectively. In order to explore the concept of deposit remediation through ash modification in coal-fired gas turbines, several tests employing inorganic additives to Blue gem coal slurry were performed. The Blue Gem coal is highly slagging, dominated by the considerable presence of iron and calcium, Table 1.

ALUMINA ADDITIVES

Alumina, Alcan A16SG 0.5 micron mass mean diameter, was added to as an aqueous dispersion to the coal slurry in an amount sufficient to double the total ash content of the fuel. Considerable care was taken to ensure that the alumina was not agglomerated in the dispersion. Combustion of the alumina-doped slurry took place for 13 hrs in the turbine simulator. During the test, the NAIN actually increased by 2%, as compared to an anticipated reduction of 2-3% for an untreated coal. The obvious implication was that erosion was occurring which was opening the critical throat region.

The test was halted after 13 hr, and the airfoils were visually inspected. Pressure side and leading edge deposits were found to be considerably less than previously obtained despite the much higher ash loading. The deposits were whitish in appearance and were only slightly fused. Signs of erosion were apparent on both the airfoils and end walls. The vane trailing edge surface had become eroded to nearly a knife edge, and bare metal was obvious along the pressure side surface. The system was reassembled and refired on oil followed by nutshelling. The abrasive injection removed virtually all leading edge and pressure side deposits, confirming the efficacy of altering ash chemistry.

The system was refired on alumina-doped coal slurry for an additional 10 hours, with reduced alumina content, now 0.5 of the indigenous 0.8% ash content. The qualitative results were identical to those observed during the initial test segment.

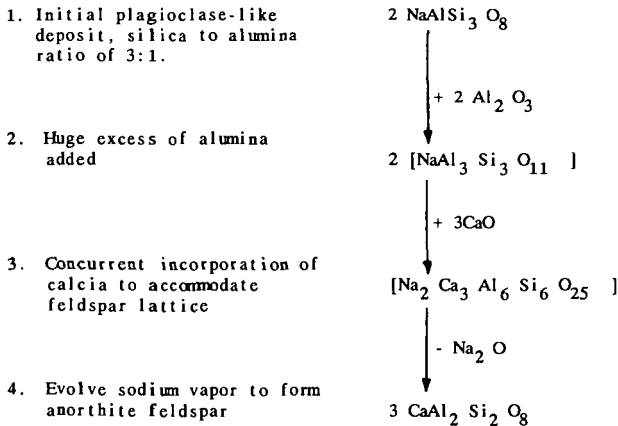
The conclusion from the alumina-added test was that indeed ash modification could take place by judicious addition of inorganic species, but that care must be taken to ensure that erosion did not occur.

BOEHMITE ADDITION

Based on the alumina test results, showing reduced ash adhesion accompanied by unacceptable erosion, boehmite was selected as an alternative. Boehmite is a hydrous alumina $\text{AlO}(\text{OH})$, isostructural with lepidochrosite. Its hardness is ca. 3.5 on Moh's scale, as compared to 9 for sapphire. Thus its erosive tendency should be greatly reduced. Further, it is available in extreme purity as a byproduct from the Ziegler process for alpha-olefin synthesis which employs triethylaluminum. The byproduct fume has an inherent particle size range in the tens of angstroms, and can be dispersed in acidic media. However, to avoid the potential for gelling, spray dried clusters 30 microns in diameter were obtained and dry-ball-milled to 0.6 microns. A slurry was prepared without dispersant, and was admixed with the coal slurry in sufficient quantity to equal the amount of indigenous ash in the coal.

The coal was burned, as usual, in the LM500 turbine simulator for a period of six hours. In contrast to the alumina test, deposition was observed with a NAIN reduction of over 1%. Large chunks formed in the transition section and on the leading edge of the airfoils, and a fine powdery adhered to the suction surfaces.

Analysis of the deposits revealed the usual complement of phases including anorthite, anhydrite, vuggy mullite crystals lining the pores, alpha alumina, hematite, and glass. Not anticipated was the presence of alkali sulfates, which we suggest arose from the following sequence:



The driving force for these reactions is to incorporate as much of the alumina into the feldspar lattice, which is also benefited by the evolution of alkali. The Si/Al ratio starts at 3/1 and ends at 1/1 as is observed. It is the evolution of alkali which results in alkali sulfate glue formation and deposition. In essence, the alumina reversed the gettingter process.

If this interpretation is correct, the use of alumina as a deposition control additive is fundamentally incorrect; it will exacerbate deposition in all but the most silica-rich deposits.

KAOLIN ADDITIVES

Kaolin clay was added, again in an amount sufficient to match the indigenous ash content of the coal. Four tests ranging from 6 to 15 hr in duration were performed using an air classified kaolin clay. Deposition on the airfoil surfaces was minimal, though upstream in the transition section leading to the

airfoils, chunks had formed which occasionally spalled and wedges in the turbine throats. Analysis of these deposits revealed a ten-fold enrichment of alkali metals in the deposit, presumably resulting from alkali impurities in the clay and the sodium polyacrylate surfactant. By using a highly beneficiated clay and an ammonium polyacrylate surfactant, the upstream deposition was considerably diminished. Comparison between deposits from the untreated coal (Figure 3) and the kaolin-treated coal (Figure 4) demonstrate clearly that it is the ash chemistry which dominates the deposition process, rather than the ash quantity.

In order to take full advantage of Kaolin for deposit mitigation, a method for eliminating formation of chunks of deposits which form in the transition piece must be identified. It is expected that through proper thermal and aerodynamic design, this will be accomplished.

It is speculated that the function of the kaolin is two-fold. First, it acts as a network extender, raising the viscosity and surface tension of the melt on the airfoils. Second, it shifts the composition of the melt from the anorthite phase field into the mullite phase field. Exsolution of the high density mullite results in pore formation, especially along the deposit/airfoil interface. The net effect is to reduce the contact area between the deposit and the airfoils so that the ash will either spontaneously spall or erode. Analytical and microscopic evidence supports this hypothesis.

SUMMARY

Deposit formation represents a key impediment to the commercialization of coal-fired gas turbines. It was determined that addition of judicious amounts of ash modifiers, especially inexpensive kaolin clays, is an effective means to render the ash non-adherent.

ACKNOWLEDGEMENTS

This work has been sponsored by the US Department of Energy, Morgantown Energy Technology Center, Contract DE-AC2186MC23168.

The authors acknowledge J. Myers of Meyers Chemical and Subash Lele of Englehard for providing additives.

REFERENCES

- [1] France, J.E., Grimm, U., Anderson, R.J., and Kovach, J.J., *DOE Report*, "Deposition and Corrosion in Gas Turbines Utilizing Coal or Coal-Derived Fuel", Report DOE/METC/84-14, 1984.
- [2] S.G.Kimura, C.L. Spiro, C.C. Chen, "Alkali Species Characterization for Coal-Fueled Gas Turbine", *Proceedings Third Annual Heat Engine Contractors Meeting*, F. Crouse, Ed., DE86001086, 92-103, 1986.
- [3] S.G.Kimura, C.L. Spiro, C.C. Chen, "Alkali Species Characterization for Coal-Fueled Gas Turbine", *Final Report*, DOE/MC/22164-2188, (1987), pp 1-39.
- [4] S.G. Kimura, C.L. Spiro and C.C. Chen, "Combustion and Deposition in Coal-Fired Gas Turbines", *ASME Journal for Engineering and Power*, Vol 109(3), 319-324 (1987). Also presented as paper 87-GT-266 at the Gas Turbine Conference and Exhibition, 5/31/87, Anaheim, CA.
- [5] S.G.Kimura, and C.L. Spiro, "Alkali Species Characterization for Coal-Fueled Gas Turbine", *Proceedings Fourth Annual Heat Engine and Gas Stream Cleanup Systems Contractors Review Meeting*, J. Byam, Jr and K.E. Markel, Jr, DE87001072, pp291-297 (1987).
- [6] F.W. Staub, S.G. Kimura, C.L. Spiro, and M.H. Horner, "Coal-Water Slurry Combustion in Gas Turbines", *Transactions of the ASME, Journal of Engineering for Gas Turbines and Power*, in

press (1988).

- [7] Kuczynski, G.C., "The Science of Sintering", *J. Scien. Sintering*, 9, 243(1977).
- [8] Raask, E., *Mineral Impurities in Coal Combustion*, Hemisphere Publishing, Washington, 1985.
- [9] K. Ross, S.G. Kimura and C.L. Spiro, *Final Report*, U.S. Department of Energy, Gas Turbine Components Screening, DoE/MC/21395-2298, (1987).
- [10] P.J. Schields, C.L. Spiro, and E. Koch, "Phase Characterization of Coal-Fueled Engine Deposits," in *Fly Ash and Coal Conversion Byproducts: Characterization, Utilization, and Disposal IV.*, edited by G.J. McCarthy, F.P. Glaser, and D.M. Roy, in press, (1988).
- [11] N. Rekos, ed., *Proceedings Sixth Annual Heat Engine Contractors Meeting*, 1988, in press.
- [12] C.L. Spiro, C.C. Chen, S.G. Kimura, "Alkali Species Characterization for Coal-Fueled Gas Turbine", *Proceedings Second Annual Heat Engine Contractors Meeting*, 149-156 (1985).
- [13] C.L. Spiro, C.C. Chen, J. Wong, S.G. Kimura, and R.B. Greeger, "Characterization of Products from a Direct Coal-Water Mixture Fired Gas Turbine Combustor", *Fuel*, 66(4), 563-567 (1987).
- [14] C.L. Spiro, S.G. Kimura, and C.C. Chen, "Ash Behavior During Combustion and Deposition in Coal Fueled Gas Turbines", *ASME Journal for Engineering and Power*, Vol 109(3), 325-330 (1987). Also presented as paper 87-GT-267 at the Gas Turbine Conference and Exhibition, 5/31/87, Anaheim, CA.
- [15] C.L. Spiro, S. G. Kimura, R.S. Lavigne, and P.J. Schields, "The Chemistry of Deposition in Coal-Fired Gas Turbines", in *Proceedings of the Mineral Matter and Ash From Coal Engineering Foundation Conference*, F. Bryers and K. Vorres, editors, in review, 1988.
- [16] Wenglarz, R.A., "Turbine Deposition, Erosion, and Corrosion Evaluations Using a Simplified Test Approach", ASME Paper 87-GT-214, Presented at the Gas Turbine Conference and Exhibition, Anaheim, CA, June, 1987.

Table 1- Properties of Otisca Coal-Water Mixture

PROXIMATE ANALYSIS (Dry Basis)		ASH ANALYSIS	
Ash Content %	0.90	SiO ₂	22.4
Total Sulfur %	0.80	Al ₂ O ₃	29.15
Volatile %	37.92	TiO ₂	1.80
Fixed Carbon %	61.18	Fe ₂ O ₃	28.54
Solids %	49.87	CaO	9.86
Viscosity cp (112/sec)	270	MgO	3.00
		K ₂ O	0.17
		Na ₂ O	0.54
		SO ₃	0.62
		P ₂ O ₅	0.33
		SrO	1.09
		BaO	0.67
		MnO	0.04

PARTICLE SIZE DISTRIBUTION

Diameter	Mass %
> 11.5	7.0
11.5	0.5
10.5	0.0
9.5	4.0
8.5	4.4
7.5	3.2
6.5	6.2
5.5	7.6
4.5	10.8
3.5	14.0
2.5	18.4
1.5	18.5
0.5	5.4

ASH FUSION DATA

	Reducing	Oxidizing
Initial Def	2215	2470
Softening	2415	2545
Hemispherical	2535	2605
Fluid	2655	2655

D50= 3.55 micron

Figure 1- Quench probe samples show char cenospheres, fume, and frozen slag spheres.

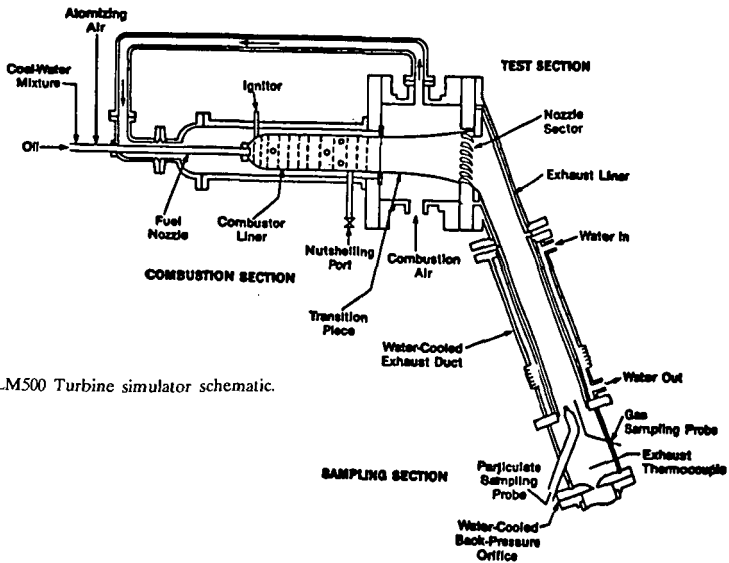
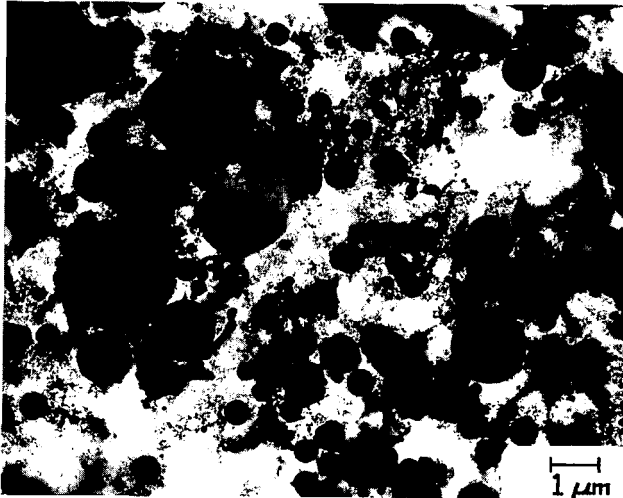


Figure 2- LM500 Turbine simulator schematic.



Figure 3- Comparison of deposition before and after treatment with kaolin additive.



A STUDY OF TECHNIQUES FOR REDUCING
ASH DEPOSITION IN COAL-FIRED GAS TURBINES

Ronald G. Logan, George A. Richards,
Charles T. Meyer, and Rodney J. Anderson
U.S. Department of Energy
Morgantown Energy Technology Center
Morgantown, WV 26505

INTRODUCTION

Corrosion and deposition on engine components are potential barriers to the utilization of coal and coal-derived fuels in heat engines. The U.S. Department of Energy has established a program to study mechanisms of ash deposition, with the goal of developing methods to alleviate deposition problems in coal-fired gas turbines. Ash deposits are formed in the turbines by the adherence of ash particles to the surfaces of stators and blades. During combustion, components of the coal ash become molten and thus readily adhere to metal surfaces in the turbine upon impaction (Figure 1) [1]. Deposit growth can be enhanced by the formation of a liquid layer on the surface of the ash particles, which may consist of alkali sulfates, aluminosilicates, or low-melting compounds of iron or calcium [2-5]. Typically, some fraction of the total amount of ash (denoted as the sticking coefficient [6,7]) actually sticks to turbine components forming a deposit.

The tendency of various coals to form ash deposits during combustion is a function of several variables including the ash chemistry, the gas temperature and pressure, the gas velocity, and the temperature of the turbine components. The objective of this work was to measure the sticking coefficient of various coals while studying the basic mechanisms of ash deposit formation to facilitate the development of techniques for preventing deposition in coal-fired gas turbines. Two methods of mitigating ash deposition were studied; active cooling of the deposition target, and the use of fuel additives. Surface cooling has been shown to be effective at reducing ash deposition in boilers [8] and in tests in gas turbine simulators [9]. Deposition reduction can also be accomplished by the use of fuel additives. The injection of additives which can promote spalling of weakly bonded ash has been used in boilers to reduce deposit strength [8]. It has been proposed that additives can act as getters for vapor phase alkali [10] to prevent the formation of low-melting alkali sulfates which can act as a glue to increase deposition. The additives may also contribute to the erosion of ash deposits. Spiro et al. [11] have reported the successful use of kaolin clay to reduce deposition problems in a gas turbine simulator.

EXPERIMENTAL

Experiments were performed in an electrically heated, laboratory scale drop-tube combustor designed to operate at temperatures up to 1500 C and pressures up to 12 atmospheres. This combustor, the combustion/deposition entrained reactor (CDER), is shown in Figure 2. The reaction zone in the CDER is 50.8 cm long and 5.1 cm in diameter. The residence time of coal particles in the reaction zone is approximately 500 ms. Approximately 3 grams per hour of -400 mesh pulverized coal was entrained in air from a circulating feeder, and injected into the reactor with a total air flow rate of 30 slpm. These fuel and air flow rates resulted in a relatively low equivalence ratio of 0.015, compared to overall

equivalence ratios of approximately 0.3 in gas turbines. However, deposition characteristics were shown to be independent of equivalence ratio for coal feed rates varied over an order of magnitude. The coal feed rate used in these experiments allowed longer sampling times which increased the ease and consistency of the measurements.

At the exit of the reaction zone the products of combustion were accelerated through a 3.2 mm diameter nozzle, creating a jet which impinged on a flat platinum disk at approximately 300 m/s, similar to the gas velocity expected in the first stage of a gas turbine. At this velocity, a stagnation flow configuration was created such that all particles greater than 0.5 microns in diameter impacted on the target, as would occur on the leading edge of a gas turbine blade. The 12.7 mm diameter platinum targets were positioned approximately 6 mm below the nozzle aperture. The nozzle and target configuration are shown in Figure 3. Platinum was used as a target material because of its inertness, thereby eliminating surface reactions peculiar to a specific blade material which could effect the experimental results. The target surface was cooled from the underside by introducing an opposing jet of cooling air. Thus the targets could be cooled over a range of temperatures by varying the cooling air flow rate. The target temperature was measured throughout each test via a two-color optical pyrometer monitoring the backside of the platinum target.

The reactor is equipped with three sets of optical access ports for use with a variety of nonintrusive diagnostic instrumentation that is currently under development. An on-line mass spectrometer was used to monitor the major components of the exhaust. A more detailed description of the CDER and its associated instrumentation has been presented previously [12].

Sticking coefficients were determined by first passing the jet of gas and ash particles through a filter to determine the total mass arrival rate. A vacuum pump was used to draw the gas through the filter, which was positioned in the same location as the target. Then a target of known weight was inserted in the jet and a deposit was collected for a specified period of time, usually 10 minutes. The sticking coefficient was calculated as the ratio of the weight gain of the target to the total mass arriving at the target (determined by the filter sample). The filter samples were quenched with cold air, resulting in unburned carbon in the samples. Since carbon was burned out of the deposits, filter samples were analyzed for carbon content to correct the ash arrival rate used to calculate the sticking coefficient.

The adhesion strength of the ash deposits was measured with an in situ adhesion strength meter (ASM). The ASM (shown in Figure 4) consists of a quartz load cell connected to a linear actuator. Attached to the linear actuator is a ceramic probe mounted on a rotational stage for precise control of the probe position. The entire unit is mounted on a precision translation stage, and the probe is coupled directly to the CDER for in situ measurements. When pressure is applied to an ash deposit via the probe, the load cell measures the shear force required to break the deposit free from the platinum target at the temperature of the reactor.

RESULTS

The baseline coal used in this study was Arkwright Pittsburgh bituminous. In addition, a highly-cleaned Kentucky Blue Gem bituminous coal was also studied.

Chemical analyses of the Arkwright and Blue Gem coals are shown in Table 1. All data reported here were collected at atmospheric pressure. Results from tests utilizing target cooling for ash deposition mitigation showed that at lower combustion (exhaust gas) temperatures (1100 C), target cooling had no effect on the sticking coefficient. However at higher combustion temperatures (1300 C), target cooling produced a significant reduction in the fraction of adhering ash (Figure 5). Sticking coefficients were higher at 1100 C and deposits were granular in character and easily removed. Deposits collected at 1300 C, although smaller, were tightly bonded to the target surface. Scanning electron microscope particle size analyses of ash samples collected at the two combustor temperatures showed that the high temperature combustion produced ash particles less than 20 microns in diameter, with a peak in the mass distribution of approximately 5 microns. Conversely, a large fraction of the low temperature ash was concentrated in the particle sizes between 10 and 40 microns. Only a small fraction of the ash was contained in particles smaller than 5 microns. It was proposed that target cooling was effective at reducing deposition at the higher combustion temperatures because the smaller particles were more easily cooled in the boundary layer above the cooled surface, which effectively froze the molten phases in the particles. The larger particles produced at the lower combustion temperature arrived at the target unaffected by the cooled surface. The data suggest that a proper combination of combustion history and hardware surface temperature can contribute to effective deposition mitigation if the combustion process is tailored to produce fine ash particles. A detailed discussion of these results has been presented elsewhere [13].

Three additives were tested; limestone and tricalcium silicate (potential sulfur sorbents), and kaolin. These additives were ground to -400 mesh and mixed with the coal prior to combustion in the CDER. Figures 6 and 7 show the effects of the addition of various amounts of kaolin on the sticking coefficient of Arkwright coal at 1100 and 1300 C, respectively. The data in Figure 6 show that the addition of kaolin had no effect at a reactor temperature of 1100 C until the amount of added kaolin roughly equaled the weight per cent of ash in the coal. Target surface cooling was ineffective at reducing the sticking coefficient at any percentage of kaolin addition for a reactor temperature of 1100 C, as was the case with the Arkwright coal alone. Figure 7 shows the results of similar tests conducted at a reactor temperature of 1300 C. At this temperature, the effectiveness of kaolin addition was more pronounced. Increasing percentages of kaolin decreased the sticking coefficient, and further, kaolin addition enhanced the mitigating effect of target cooling. In fact, the sticking coefficient measured with 7.5 percent kaolin addition and maximum target cooling was the lowest recorded for the Arkwright coal under any reactor conditions or with any other additive tested. This sticking coefficient was approximately an order of magnitude lower than that of the Arkwright coal alone with cooled targets and approximately two orders of magnitude lower than Arkwright alone with no cooling of the target surface.

Limestone addition reduced the sticking coefficient by an order of magnitude at a reactor temperature of 1100 C, and to a lesser degree at a temperature of 1300 C (Figures 8 and 9). However, cooling the deposition target had no effect on the sticking coefficient at either reactor temperature. This is in contrast to results of tests with Arkwright coal only, and Arkwright plus kaolin which showed an order of magnitude reduction in sticking with target cooling at a reactor temperature of 1300 C. Tests with tricalcium silicate produced results similar to those for the limestone tests. Tricalcium silicate was more effective at 1100 C (Figure 10). At a Ca/S ratio of 4, the sticking coefficient was

reduced approximately an order of magnitude, however there was no effect of target cooling. At a reactor temperature of 1300 C with Ca/S ratios less than 1.0, the deposition characteristics were similar to Arkwright coal only, showing an order of magnitude decrease with target cooling (Figure 11). However, mixtures with higher Ca/S ratios showed no reduction of sticking coefficient with target cooling.

The addition of kaolin substantially reduced the adhesion strength of the ash deposits. Many of the deposits collected during the kaolin tests fell off of the targets as they were removed from the CDER. Thus, the measure of the sticking coefficient alone may not adequately assess the effectiveness of kaolin addition for deposition reduction, since the fraction of ash that does adhere is easily removed. Kaolin may react chemically with components of the ash to produce a more friable deposit [10]. Deposits collected during limestone and tricalcium silicate addition lacked this feature, indicating that sticking coefficient reductions measured during these tests may have been due to deposit erosion.

CONCLUSIONS

In general, tricalcium silicate and limestone were marginally effective at reducing the sticking coefficient of the coal at the lower reactor temperature. Both additives tended to reduce the effectiveness of target cooling for lowering the sticking coefficient. Thus, while limestone addition lowered the sticking coefficient at 1300 C with no target cooling, the sticking coefficient was lower without the additive when the target was cooled. Kaolin was very effective at reducing both the sticking coefficient and the adhesion strength of the ash deposits, and produced the lowest sticking coefficient measured for the baseline coal. The data showed that the proper combination of gas temperature, surface temperature, and additive can be an effective means of minimizing the detrimental effects of ash deposition in coal-fired gas turbines.

REFERENCES

1. France, J. E., U. Grimm, and R. J. Anderson, "Deposition and Corrosion in Gas Turbines Utilizing Coal or Coal-Derived Fuels," DOE/METC/84-17 (DE84009290), (1984).
2. Cross, N. L., and R. G. Picknett, "Particle Adhesion in the Presence of a Liquid Film," The Mechanism of Corrosion by Fuel Impurities, H. R. Johnson and D. J. Littler. eds., Butterworths, London, pp. 383-390 (1963).
3. Wibberly, L. J., and T. F. Wall, "Alkali-Ash Reactions and Deposit Formation in Pulverized Coal-Fired Boilers: The Thermodynamic Aspects Involving Silica, Sodium, Sulfur, and Chlorine," Fuel, 61, 87-92 (1982).
4. Wibberly, L. J., and T. F. Wall, "Alkali-Ash Reactions and Deposit Formation in Pulverized Coal-Fired Boilers: Experimental Aspects of Sodium Silicate Formation and the Formation of Deposits," Fuel, 61, 93-99 (1982).
5. Wibberly, L. J., and T. F. Wall, "Deposit Formation and Sticky Particles from Alkali-Ash Reactions, Fouling and Slagging Resulting from Impurities in Combustion Gases, R. W. Breyers, ed., Engineering Foundation, New York, New York, pp. 493-513 (1983).

6. Rosner, D. E., and R. Nagarajan, "Toward a Mechanistic Theory of Net Deposit Growth from Ash-Laden Flowing Combustion Gases: Self-Regulated Sticking of Impacting Particles and Deposit Erosion in the Presence of Vapor Deposited or Submicron Mist 'Glue'," AIChE Symposium Series, Heat Transfer -- Pittsburgh, No. 257, 83, (1987).
7. Ross, J. S., and R. J. Anderson, "Effect of Sodium on Deposition in a Simulated Gas Turbine Environment," J. Energy & Fuels, 2, p. 282, (1988).
8. Raask, E., Mineral Impurities in Coal Combustion: Behavior, Problems, and Remedial Measures, Hemisphere Publishing Corporation, Washington, D.C., (1985).
9. Ahluwalia, R. K., K. H. Im, and R. A. Wenglarz, "Flyash Adhesion in Simulated Coal-Fired Gas Turbine Environment," ASME Paper GT-135 Presented at the Gas Turbine and Aeroengine Congress and Exposition, Amsterdam, The Netherlands, June 5-9, 1988.
10. Scandrett, L. A., and R. Clift, "The Thermodynamics of Alkali Removal from Coal-Derived Gases," Journal of the Institute of Energy, 391 (1984).
11. Spiro, C. L., C. C. Chen, S. G. Kimura, R. S. Lavigne, and P. J. Schields, "Deposit Remediation in Coal-Fired Gas Turbines Through the Use of Additives," To Be Presented at the 197th Annual Meeting of the American Chemical Society, Dallas, Texas, April 9-14, 1989.
12. Anderson, R. J., C. T. Meyer, and R. A. Dennis, "A Combustion/Deposition Entrained Reactor for High Temperature/Pressure Studies of Coal and Coal Minerals," To be presented at the 1988 Annual AIChE Meeting, Washington, D.C., November 1988.
13. Richards, G. A., R. G. Logan, C. T. Meyer, and R. J. Anderson, "Ash Deposition Temperature Effects," Submitted for publication in Transactions of the ASME, (1988).

Coal Rank	Arkwright Pittsburgh Bituminous	Blue Gem (Cleaned) Bituminous
% ASTM Ash	6.93	0.56
Ash Comp. (Wt%)		
SiO ₂	48.09	16.86
Al ₂ O ₃	25.07	22.75
Fe ₂ O ₃	10.95	29.57
TiO ₂	1.27	1.95
P ₂ O ₅	0.18	0.48
CaO	5.78	7.03
MgO	1.25	2.46
K ₂ O	1.16	0.53
Na ₂ O	0.90	1.54
SO ₂	5.34	8.07
Ash Fusion Temp. (C) (± 40)		
(ASTM, 1977)		
Initial Deformation	1,190	1,238
Softening	1,316	1,308
Hemispherical	1,356	1,371
Fluid	1,383	1,427

Table 1: Ash Characteristics

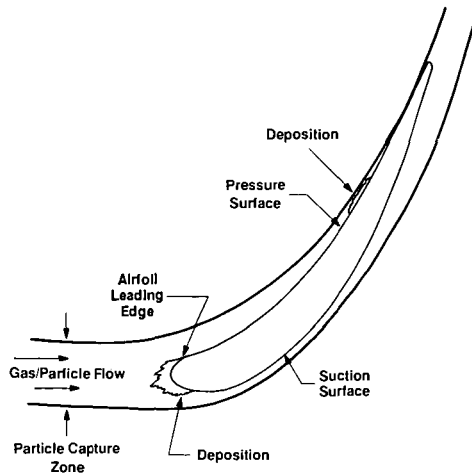


Figure 1: Particle Deposition on a Gas Turbine Vane

Item	Test Section
PRESSURE, ABSOLUTE, atm	1-12
FLOW RATE, scfh	25-700
VESSEL LENGTH, in	60
VESSEL OUTSIDE DIAMETER, in	24
WALL THICKNESS, in	1/4 (sch 40-304LSS)
PROCESS STREAM EXIT TEMPERATURE, °F	2,500
VESSEL SKIN TEMPERATURE, °F	< 300
ELEMENTAL TEMPERATURE (maximum), °F	3,000
HEATING ELEMENTS	KANTHAL SUPER 33 9/18
HEATER OUTPUT, watts	7,060
POWER SUPPLY, V/IA	35/350
EXHAUST FLOW COMPOSITION	DILUTE COAL POC/ FILTERED
EXHAUST FLOW PRESSURE/TEMPERATURE	< 2 atm; < 400°F

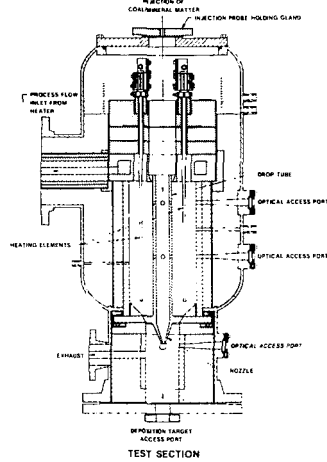


Figure 2: CDER System Design Specifications

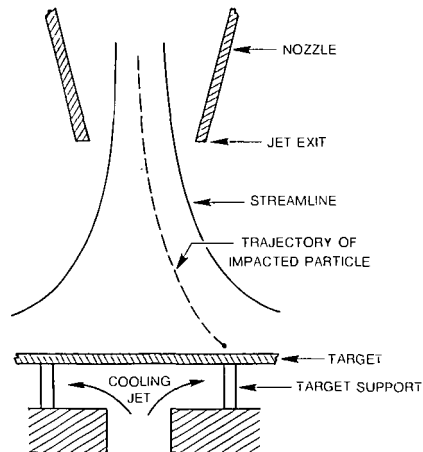


Figure 3: CDER Nozzle/Target Assembly

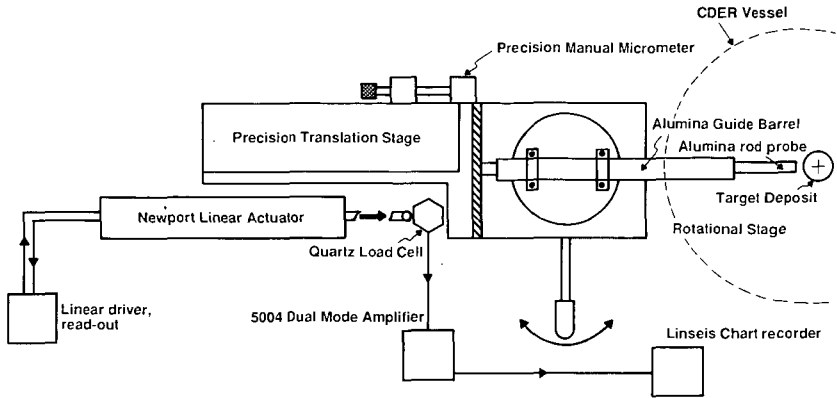


Figure 4: Adhesion Strength Meter (ASM)

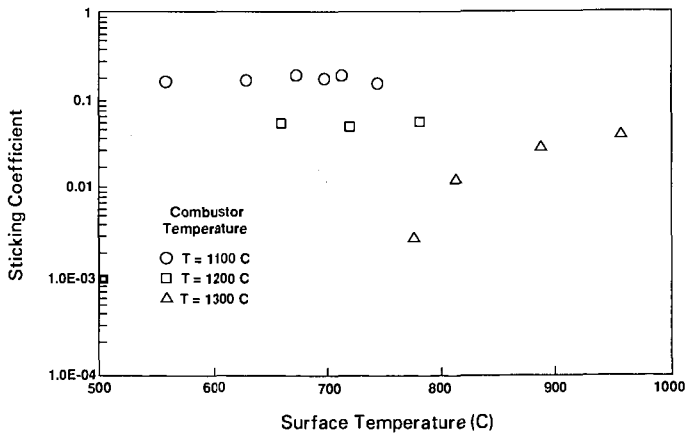


Figure 5: Effect of Target Cooling on Deposition; Arkwright Coal

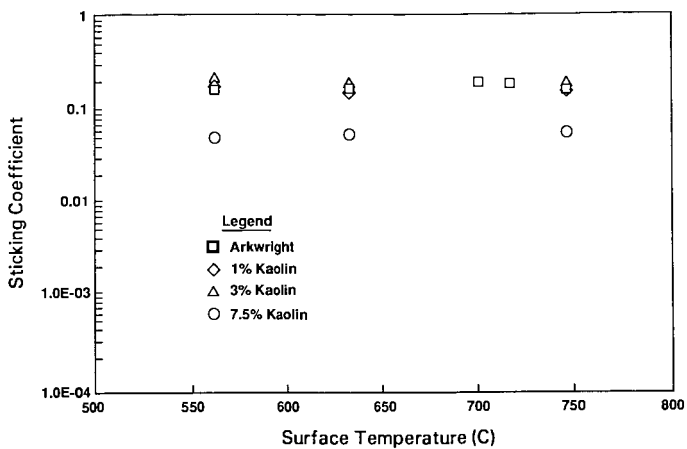


Figure 6: Effect of Target Cooling on Deposition; Arkwright Coal/Kaolin, T=1100 C

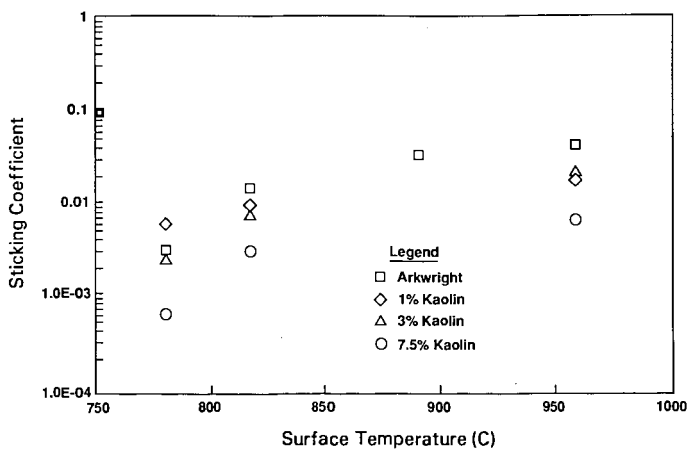


Figure 7: Effect of Target Cooling on Deposition; Arkwright Coal/Kaolin, T=1300 C

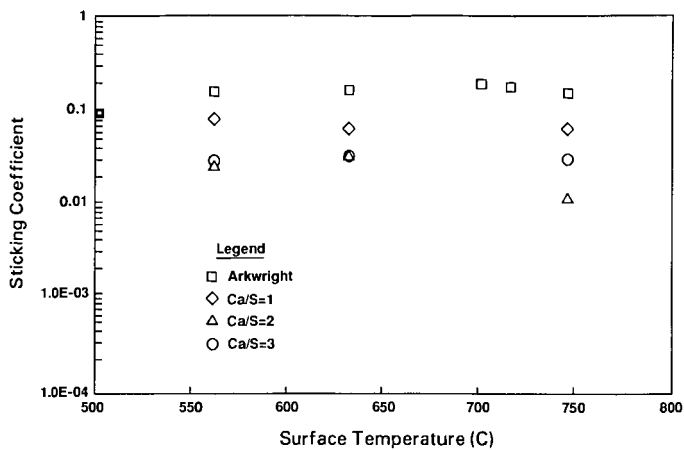


Figure 8: Effect of Target Cooling on Deposition; Arkwright/Limestone, T=1100 C

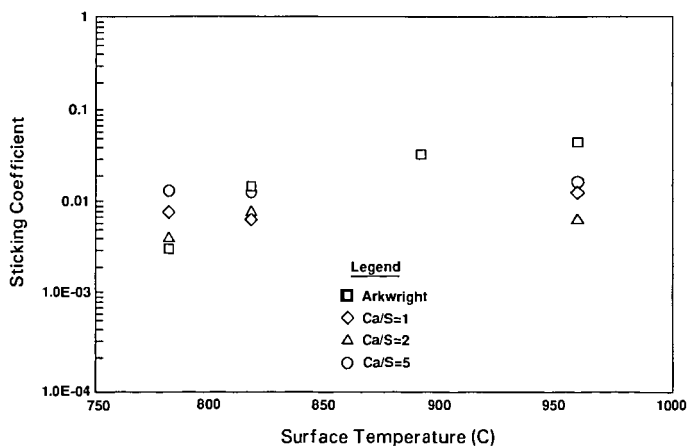


Figure 9: Effect of Target Cooling on Deposition; Arkwright/Limestone, T=1300 C

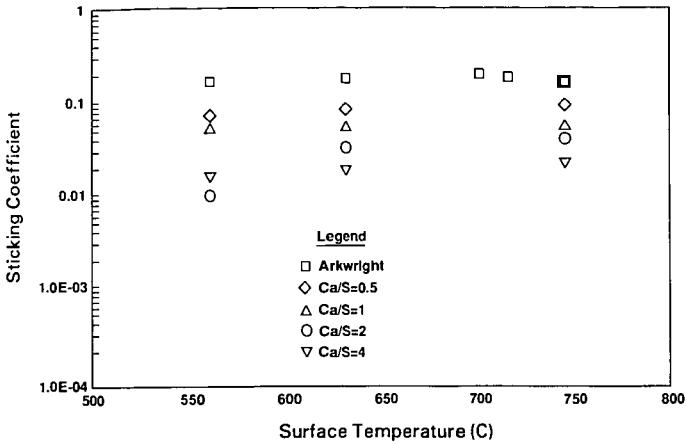


Figure 10: Effect of Target Cooling on Deposition; Arkwright/Tricalcium Silicate, T=1100 C

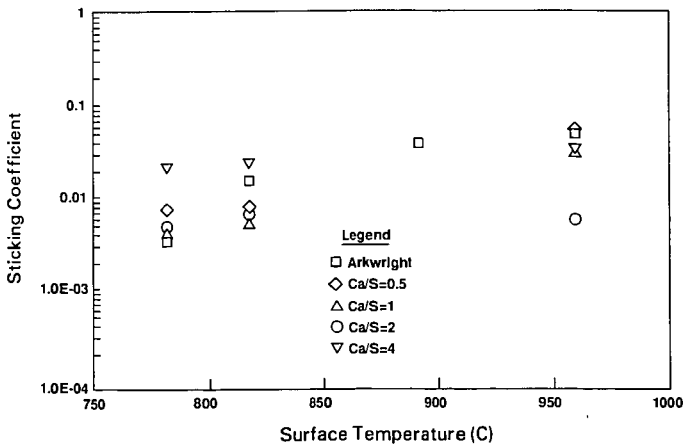


Figure 11: Effect of Target Cooling on Deposition; Arkwright/Tricalcium Silicate, T=1300 C

PHOTOPHORETIC CONTRIBUTION TO THE TRANSPORT OF ABSORBING PARTICLES ACROSS COMBUSTION GAS BOUNDARY LAYERS¹

Jose L. Castillo², Daniel W. Mackowski³, and Daniel E. Rosner⁴
Yale University, Department of Chemical Engineering
High Temperature Chemical Reaction Engineering Laboratory
New Haven, CT 06520, U.S.A

Abstract

Since radiation energy fluxes can be comparable to 'convective' (Fourier) fluxes in large fossil-fuel-fired power stations and furnaces, we have examined particle drift ('phoresis') induced by nonuniform photon-particle heating in a 'host' gas. Our analysis (Mackowski, 1988) of the photophoretic velocity includes the important 'slip-flow' regime, and the numerical results show that photophoresis is a significant transport mechanism for micron-sized absorbing particles in high radiative transfer combustion environments, with equivalent photophoretic diffusivities (dimensionless photophoretic velocities) being as large as 10 percent of the better-known thermophoretic diffusivity (Rosner, 1980, 1985). Since previous experimental results (Rosner and Kim, 1984) demonstrated that thermophoresis causes over a 3-decade increase in particle deposition rates by convective diffusion, clearly, for small, absorbing particles, photophoresis will also be an important contributor to observed deposition rates. Accordingly, we present mass transfer coefficients for particle transport across laminar gaseous boundary layers, including both particle thermophoresis and photophoresis.

Thermophoresis and Photophoresis

When both radiative and convective energy fluxes are present in a gas environment with a dilute amount of aerosol particles, the motion of these particles is affected by temperature gradients in two different ways.

Thermophoresis describes the phenomenon wherein small particles in a gas experience a force in the direction opposite to the thermal gradient in the gas. The thermophoretic velocity (*i.e.*, the terminal velocity reached for an isolated particle in a gas with a constant temperature gradient) is normally written in the form:

$$\vec{v}_{th} = \alpha_T \left[\frac{-(\text{grad } T)}{T} \right] \quad [1]$$

where α_T is a dimensionless thermal diffusion factor and D_p the diffusion coefficient of the particles. Actually, D_p is included here just to emphasize the similarity between \vec{v}_{th} and a diffusion

¹ Research supported, in part, by the U.S. DOE PETC under grant DE-FG22-86FC90756. To be presented to the 197th Annual ACS Mtg., Symposium on Ash Deposition, Dallas-TX, April 9-14. DER#171

² Professor and Head, Depto. Fisica Fundamental, U.N.E.D., Madrid, Spain

³ Postdoctoral Research Associate, Yale University, Chemical Engineering Dept., HTCRES Laboratory.

⁴ Professor of Chemical Engineering, Yale University, Chemical Engineering Dept.; Director, HTCRES Laboratory, to whom all inquiries concerning this research should be directed.

velocity, but the value of the thermophoretic diffusivity $\alpha_T D_p$ does not really depend on D_p (which, in fact, will be taken to be zero in our analysis). Talbot *et al.* (1980), presented an expression for $\alpha_T D_p$:

$$\alpha_{th} D_p = \frac{2c_s v \left(\frac{K_g}{K_p} + c_t \frac{l}{a} \right) \left[1 + \frac{l}{a} (A + B e^{-Ga/l}) \right]}{\left(1 + 3 c_m \frac{l}{a} \right) \left(1 + 2 \frac{K_g}{K_p} + 2c_t \frac{l}{a} \right)} \quad [2]$$

where K_g and K_p are the thermal conductivities of the gas and particle, respectively; l is the gas mean-free path, $l=2v/\bar{c}$, with $\bar{c}=(8RT/\pi)^{1/2}$; a is the particle radius, $A=1.20$, $B=0.41$, $G=0.88$, and, for perfect accommodation between the particle and the gas molecules, $c_s=1.17$, $c_m=1.1$ and $c_t=2.18$; v is the gas kinematic viscosity.

Note that, in the limit of $K_p \geq K_g$ and $a \ll l$, Eq. [1.2] reduces to:

$$\alpha_{th} D_p \cong \frac{c_s v}{3c_m} (A + B) \cong 0.56 v$$

(the numerical factor in Waldmann's theory, 1961, is 0.54). This simple limiting case provides a first approximation for the magnitude of $\alpha_{th} D_p$, and motivates our introduction of $\alpha \equiv \alpha_{th} D_p / v$ in the analysis and examples which follow.

On the other hand, photophoresis takes into account the particle motion induced by the temperature gradient upon the particle surface originating from the nonuniform absorption of the radiant energy within the particle. The correspondent photophoretic velocity for an isolated particle can be written as

$$\vec{v}_{ph} = \alpha_{ph} D_p \frac{\vec{q}_R}{K_g T} \quad [3]$$

where $\alpha_{ph} D_{ph}$ is the photophoretic diffusivity and \vec{q}_R the radiative heat flux. Mackowski (1988) obtained an expression for \vec{v}_{ph} in the slip flow regime, resulting in

$$\alpha_{ph} D_p = -\frac{2c_s v \bar{J}_1}{3} \frac{1 + \frac{l}{a} (A + B e^{-Ga/l})}{\left(1 + 3 c_m \frac{l}{a} \right) \left(1 + 2c_t \frac{l}{a} + 2 \frac{K_g}{K_p} \right)} \quad [4]$$

whereas in the free molecular limit

$$\alpha_{ph} D_p = -0.14 v \bar{J}_1 \frac{a}{l} \quad [5]$$

\bar{J}_1 is the thermophoretic asymmetry factor and represents a weighted integration of the absorption of radiant energy over the particle volume. For spherical, homogeneous particles and monochromatic radiation, \bar{J}_1 can be obtained from Lorenz-Mie theory as a function of the particle radiative size parameter $\chi=2\pi a/\lambda$, where λ is the radiation wavelength, and the complex index of refraction $m=n+ik$. An exact, series-expansion expressions for \bar{J}_1 has been derived which is analogous to the expressions for the radiative cross sections (Mackowski, 1988). For spectrally-distributed radiation, \bar{J}_1 is obtained from integration over the wavelength distribution.

Realize that \bar{J}_1 can be positive or negative, leading to \bar{v}_{ph} directed either against or with the incident radiation direction. For radiation absorbed entirely on the particle surface, \bar{J}_1 attains a minimum value of -0.5 .

Underlying Assumptions

To simplify the problem without losing its essential features, the following defensible assumptions will be made:

- A1. The flow within the BL is steady and laminar. The usual BL approximations will be used and self-similarity will be assumed (see, *e.g.*, Schlichting, 1968).
- A2. The aerosol particles are very dilute so that the prevailing velocity and temperature field are not affected by their presence.
- A3. All thermophysical properties of the gas will be considered constant and equal to the values for the carrier gas at mainstream conditions. Transport properties for the dispersed aerosol will also be taken to be constant. Lastly, the system will be considered effectively incompressible, *i.e.*, the density will be assumed to be constant.
- A4. Aerosol particles do not appreciably Brownian diffuse. Therefore, at each position, the velocity of the particles is taken to be the gas velocity plus the thermophoretic and photophoretic velocities, with these velocities being those corresponding to an isolated particle in a uniform gas with the same temperature gradient and radiant energy flux. The direction of the radiative flux will be taken along the normal to the solid collecting surface.

We consider the two-dimensional stagnation point (Hiemenz) flow. This corresponds to a steady flow which arrives from the y -axis, impinges on a flat solid wall placed at $y=0$, where it divides into two streams near the wall, leaving in both (\pm) directions. The external (inviscid) velocity distribution in the neighborhood of the symmetrical forward stagnation "point" (at $x=y=0$) is given by (*e.g.* Schlichting, 1968):

$$u_e(x) = \left(\frac{du_e}{dx} \right)_{x=0} \cdot x \quad [6]$$

In the immediate vicinity of the solid wall, viscous (momentum diffusion) effects become important and, for a Newtonian fluid, the velocity field must satisfy the well-known two-dimensional BL equations:

$$u \frac{\partial u}{\partial x} + v \frac{\partial u}{\partial y} = u_e \frac{\partial u_e}{\partial x} + \nu \frac{\partial^2 u}{\partial y^2} \quad [7]$$

and

$$\frac{\partial u}{\partial x} + \frac{\partial v}{\partial y} = 0 \quad [8]$$

with boundary conditions: $u=0$ (no slip) and $v=0$ (no blowing) at $y=0$ and $u = u_e(x)$ at $y=\infty$.

Introducing the "stretched" dimensionless coordinate

$$\eta \equiv y \left[\frac{1}{\nu} \left(\frac{du_e}{dx} \right)_{x=0} \right]^{1/2} \quad [9]$$

and a stream function given by

$$\psi(x, y) = \left[\nu \left(\frac{du_e}{dx} \right)_{x=0} \right]^{1/2} \cdot f(\eta) \cdot x \quad [10]$$

the equation of local mass conservation [8] is automatically satisfied and the velocity components become

$$u = \frac{\partial \psi}{\partial y} = u_e(x) \cdot f'(\eta) \quad [11]$$

and

$$v = -\frac{\partial \psi}{\partial x} = - \left[\nu \left(\frac{du_e}{dx} \right)_{x=0} \right]^{1/2} \cdot f(\eta) \quad [12]$$

where above, and in what follows, primes denote differentiation with respect to η . Introducing these expressions into the x -momentum balance, equation [7], the following well-known nonlinear third-order (Blasius) ODE for $f(\eta)$ is obtained:

$$f''' + ff'' + [1 - (f')^2] = 0 \quad [13]$$

with the boundary conditions:

$$f = f' = 0 \quad @ \quad \eta = 0 \quad [14]$$

$$f' = 1 \quad @ \quad \eta = \infty \quad [15]$$

Notice that our assumptions of constant thermophysical properties and low mass loading allow $f(\eta)$ to be determined independently of the temperature and mass-fraction fields discussed below. Indeed, we will make use of the previous numerical computations of this well-known (Blasius) function (Schlichting, 1968).

Temperature Field

In the steady state, using laminar BL approximations A1, the PDE which governs the temperature distribution $T(x, y)$ is

$$u \frac{\partial T}{\partial x} + v \frac{\partial T}{\partial y} = \alpha_h \frac{\partial^2 T}{\partial y^2} \quad [16]$$

α_h being the heat (thermal) diffusivity. Defining

$$\theta \equiv \frac{T - T_w}{T_\infty - T_w} \quad [17]$$

when the wall temperature, T_w , is held constant, the ODE for $\theta(\eta)$ becomes

$$\theta'' + \text{Pr} \cdot f(\eta) \cdot \theta' = 0 \quad [18]$$

subject to the boundary conditions

$$\theta(\zeta) \equiv \theta_w = \frac{T_w}{T_\infty}, \quad \theta(\infty) = 1 \quad [19]$$

where Pr is the host gas Prandtl number, ν/α_h . The solution can be written in the following quadrature form (e.g. Spalding & Evans, 1961):

$$\theta(\eta) = \theta_w + (1 - \theta_w) \cdot \frac{1}{\delta_T} \int_0^\eta \exp\left[-\text{Pr} \int_0^\xi f(\xi) d\xi\right] d\phi \quad [20]$$

where $f(\eta)$ is defined by [13]-[15] and

$$\delta_T \equiv \int_0^\infty \exp\left[-\text{Pr} \int_0^\xi f(\xi) d\xi\right] d\phi \quad [21]$$

For a description of the computation of δ_T see, for example, Castillo & Rosner (1988), Section 3.1. For $\text{Pr}=0.7$ (e.g. air) we find $\delta_T=2.01669$.

Particle Number Density

Now consider that in the mainstream there are $N_{p,\infty}$ particles per unit volume, each with the same radius⁵, a_∞ . In the absence of particle coagulation or break-up, the number density of particles N_p satisfies the equation

$$\text{div}(\vec{v}_p N_p) = 0 \quad [22]$$

Under assumption A4., the local particle velocity is given by

$$\vec{v}_p = \vec{v} + \vec{v}_{ph} + \vec{v}_{th} \quad [23]$$

with \vec{v}_{ph} and \vec{v}_{th} given by Eq.[3] and Eq.[1], respectively. Defining $n \equiv N_p/N_{p,\infty}$, the first ODE for n takes the simple form

$$A \frac{dn}{d\eta} + Bn = 0 \quad [24]$$

where we have introduced the dimensionless functions

$$A(\eta) \equiv f(\eta) + \frac{1}{\theta} \left(\beta + \alpha \frac{d\theta}{d\eta} \right) \quad [25]$$

$$B(\eta) \equiv \frac{d}{d\eta} \left(\frac{1}{\theta} \left(\beta + \alpha \frac{d\theta}{d\eta} \right) \right) \quad [26]$$

with

$$\alpha \equiv \frac{\alpha_{th} D_p}{\nu} \quad [27]$$

$$\beta \equiv -\frac{\alpha_{ph} D_p \rho R}{K_g T_\infty} \left[\left(\frac{du_e}{dx} \right)_{x=0} \nu \right]^{-1/2} \quad [28]$$

⁵ This assumption may easily be relaxed in order to deal with a distribution of particle sizes in the main stream.

The solution of Eq.[24], with boundary condition $n=1$ @ $\eta=\infty$, can be written in the form of a quadrature

$$n = \exp \left[\int_{\eta}^{\infty} \frac{B(\varphi)}{A(\varphi)} d\varphi \right] \quad [29]$$

The normal velocity of particles within the boundary layer is given by

$$v_p = v + v_{th} + v_{ph} = - \left[v \left(\frac{du_c}{dx} \right)_{x=0} \right]^{1/2} \left[f + \alpha \left(\frac{d \ln \theta}{d \eta} \right) + \frac{\beta}{\theta} \right] \quad [30]$$

which is negative for particles approaching the wall.

Under some circumstances, the particles do not arrive to the wall and a dust free region appears inside the boundary layer (Goren, 1977). The separation line between the region with particles and the dust free zone is located at the value of η where $v_p=0$; that is

$$A = f + \frac{1}{\theta} \left(\beta + \alpha \frac{d\theta}{d\eta} \right) = 0$$

When thermophoresis and photophoresis both push the particles away from the wall, that is, when $\theta_w > 1$ and $\beta < 0$, the dust free zone will exist for any value of β and θ_w and particles will not be collected by the solid surface. On the other hand, when both transport mechanisms compete in bringing particles towards the wall, the dust free zone exists only when

$$-\beta \geq \frac{\alpha}{\delta} (1 - \theta_w) \quad \text{for } \beta < 0 \quad \text{and } \theta_w < 1$$

or

$$\frac{\alpha}{\delta} (\theta_w - 1) \geq \beta \quad \text{for } \beta > 0 \quad \text{and } \theta_w > 1$$

Note that when both transport velocities oppose each other and are exactly equal, in modulus, at the wall (i.e., when the equal sign is verified in the above inequalities), the separation line coincides with the wall; that is, the deposition of particles vanishes even when the particles are everywhere inside the boundary layer. In this very particular case, however, some deposition will occur due to Brownian diffusion.

Anyway, here we are mainly interested in the cases when none of the above inequalities holds and deposition of particles takes place. When the particles arrive to the wall, the deposition rate of particles is given by

$$-N_w v_{p,w} = \left[v \left(\frac{du_c}{dx} \right)_{x=0} \right]^{1/2} N_{\infty} \frac{n_w}{\theta_w} \left[\beta + \frac{\alpha}{\delta} (1 - \theta_w) \right] \quad [31]$$

Thus, the dimensionless capture fraction, S , of particles will be

$$S \equiv \frac{-N_w v_{p,w}}{N_{\infty} \left[v \left(\frac{du_c}{dx} \right)_{x=0} \right]^{1/2}} = \frac{n_w}{\theta_w} \left[\beta + \frac{\alpha}{\delta} (1 - \theta_w) \right] \quad [32]$$

When we are interested in mass deposition rate instead of particle deposition, the relevant parameter is

$$J_m = \frac{1}{\rho \omega_\infty} \left[v \left(\frac{du_x}{dx} \right)_{x=0} \right]^{1/2} (-j_{m,w}) \quad [33]$$

where ω_∞ is the mass fraction of particles at mainstream and $(-j_{m,w})$ is the mass deposition rate at the wall. It is easy to see that $J_m=S$. When we consider the more practical case of a distribution of particle sizes at mainstream, the definition [33] is still valid, now with ω_∞ and $j_{m,w}$ taking into account the contribution of the different sizes. In that case, it results in

$$J_m = \frac{\int N_\infty(a) a^3 S(a) da}{\int N_\infty(a) a^3 da} \quad [34]$$

with $S(a)$ given by [32] and n_w , β and α being functions of the particle radius a .

Results for Simultaneous Photophoresis and Thermophoresis

Figure 1 represents the dimensionless capture fraction, S , as a function of the ratio T_w/T_∞ , for particles having a thermophoretic coefficient $\alpha=0.5$ (a value close to the free molecular limit). The line for $\beta=0$ corresponds to pure thermophoretic deposition with negligible photophoretic transport. In that case, particles are captured only by cold surfaces (*i.e.* when $T_w/T_\infty < 1$) and the deposition rate increases as the wall temperature decreases. When photophoresis helps to bring the particles towards the surface (*i.e.* when $\beta > 0$), it produces two effects: on one hand, it allows the capture of particles even for moderate hot surface ($T_w/T_\infty > 1$) and on the other hand it considerably increases the value of S for a given value of the ratio T_w/T_∞ . The opposite is true for negative values of β , the range of temperatures over which deposition occurs is diminished as well as the deposition rate for a given temperature. Analogous results are obtained for $\alpha=0.1$ (Figure 2) although the relative importance of photophoresis is higher. Thus, for $\beta=-10^{-1}$, no deposition occurs for the entire range of temperatures considered.

From Eq.[28], it can be seen that

$$\beta = \frac{1 - \theta_w}{\delta} \left(\frac{q_R}{q_F} \right) \alpha F^c$$

where q_F is the conductive (Fourier) heat flux at the solid surface, and F is the ratio v_{ph}/v_{th} computed for equal q_R and q_F . For particles in the slip-flow regime ($l/a < 1$), F can be expressed by

$$F = \frac{\bar{J}_1 K_g}{3 K_p \left(\frac{K_g}{K_p} + c_1 \frac{l}{a} \right)}$$

Numerical results of F for carbonaceous char and fly-ash particles exposed to a black body radiation spectrum at $T_{\text{Rad}}=1800\text{K}$ have been presented by Mackowski (1988) and are reproduced in Fig.3.

By using the above expression for β together with the values of F indicated in Fig.3, the deposition rate of char particles has been obtained and it is represented in Figure 4 for a fixed value of $T_w/T_\infty=0.7$ and different ratios of q_R/q_F . For vanishing radiative fluxes the larger char particles are more efficiently captured due to their larger thermophoretic coefficient α (obtained from Eq.[2]). When the radiative heat flux is directed from the solid surface towards the bulk (*i.e.*, when $q_R<0$), the char particles are rejected by photophoresis and the deposition rate decreases. For very large radiative fluxes, photophoresis precludes the capture of char particles larger than a given size.

It is evident from these illustrative examples that the combination of photophoresis and thermophoresis induces a change in the size distribution in the mainstream through the dependence of α and β on particle size. By an appropriate combination of radiative and conductive fluxes, particle sizes larger than a given value can be avoided in the deposit and, for particles which present an extremal in the function $F(a/l)$ (as it is the case for fly ash particles) only a narrow width of particle sizes can be selected to deposit.

References

- Castillo J.L., & Rosner D.E. (1988), "Theory of Surface Deposition from a Unary Dilute Vapor Containing Stream Allowing for Condensation within the Laminar Boundary Layer", *Chemical Engineering Science* (in press)
- Goren S.L. (1977), "Thermophoresis of Aerosol Particles into Laminar Boundary Layer on a Flat Plate", *J. Colloid Interface Science* **61**, pp.77-85
- Mackowski D.W. (1988), "Photophoresis of Aerosol Particles in the Free Molecular and Slip-Flow Regimes", *Int'l J. Heat Mass Transfer* (in press)
- Rosner D.E. (1980), "Thermal (Soret) Diffusion Effects on Interfacial Mass Transport Rates", *J. PhysicoChemical Hydrodynamics* **1**, pp.159-185
- Rosner D.E. (1985), "Mass Transfer across Gas Thermal Boundary Layers — Power Production and Materials Processing Implications", in *Heat Transfer in Fire and Combustion Systems*, HTD 45 (Law C.K. *et al.* eds.) ASME, N.Y.-N.Y., pp.3-8
- Rosner D.E. & Kim S.S. (1984), "Optical Experiments on Thermophoretically Augmented Submicron Particle Deposition from 'Dusty' High Temperature Gas Flows", *The Chemical Engineering J.* **29**, No.3, pp.147-157
- Schlichting H. (1968), *Boundary Layer Theory*, McGraw-Hill (6th ed.)
- Spalding D.B. & Evans M.L. (1961), "Mass Transfer through Laminar Boundary Layers — 3", *Int'l J. Heat Mass Transfer* **2**, pp.314-341
- Talbot L., Cheng R.K., Schefer R.W. & Willis D.R. (1980), "Thermophoresis of Particles in a Heated Boundary Layer", *J. Fluid Mechanics* **101**, pp.737-758
- Waldmann L. (1961), in *Rarefied Gas Dynamics* (Talbot L., ed.) Academic Press p.323

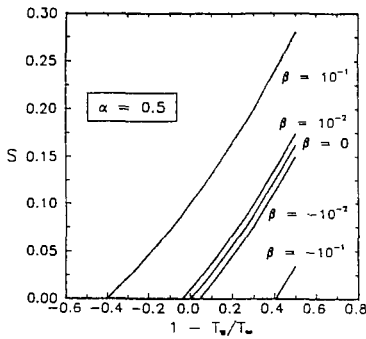


Figure 1. Dimensionless deposition rates S of particles as a function of $1-T_w/T_\infty$, for a constant thermophoretic coefficient $\alpha=0.5$ and different values of the photophoretic coefficient β .

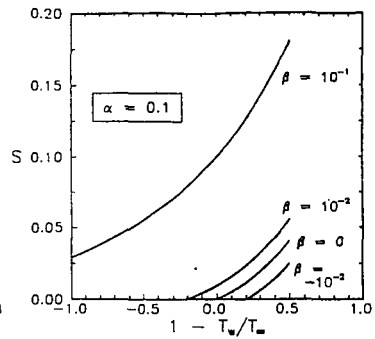


Figure 2. Dimensionless deposition rates S of particles as a function of $1-T_w/T_\infty$, for a constant thermophoretic coefficient $\alpha=0.1$ and different values of the photophoretic coefficient β .

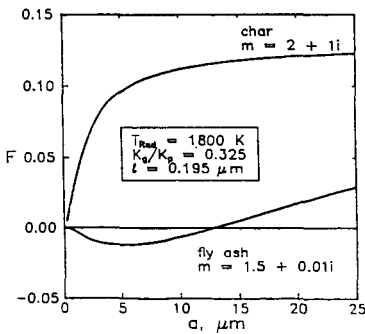


Figure 3. Photophoretic to thermophoretic velocity ratio for equal radiative and conductive heat flux, F , for carbonaceous char and fly-ash particles, as a function of particle radius. Radiation temperature $T_{Rad}=1800K$.

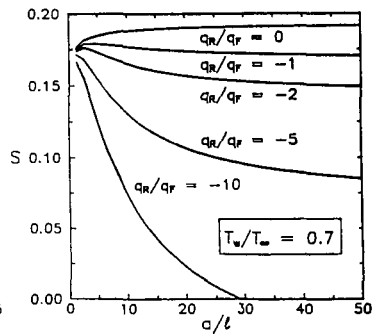


Figure 4. Dimensionless deposition rates S of char particles as a function of a/ℓ , for $T_w/T_\infty=0.7$ and different ratios of the radiative to conductive heat flux at the surface.